SIN-CHN SCIENTIFIC PRESS PTE.LTD.

Molecular & Cellular Biomechanics 2024, 21(1), 449.
https://doi.org/10.62617/mcb.v21i1.449

Article

Inverse dynamics analysis of 4-DOF stacking robot with closed chain structure

Liang Yu[1,2,3], Ronaldo Juanatas[3], Mingliang Zheng[1,2,*]

[1] Mechanical and Electrical Engineering, Huainan Normal University, Huainan 232038, China
[2] Human-computer Collaborative Robot Joint Laboratory of Anhui Province, Huainan 232038, China
[3] Technological University of the Philippines, Manila 0900, Philippines
*** Corresponding author:** Mingliang Zheng, zhmlwxcstu@163.com

CITATION

Yu L, Juanatas R, Zheng M. Inverse dynamics analysis of 4-DOF stacking robot with closed chain structure. Molecular & Cellular Biomechanics. 2024; 21(1): 449. https://doi.org/10.62617/mcb.v21i1.449

ARTICLE INFO

Received: 28 September 2024
Accepted: 22 October 2024
Available online: 25 October 2024

Abstract: A four-degree-of-freedom PR1300 stacking robot with two parallel quadrilateral structures connected in series at the shoulder was designed. The hybrid robot with local closed chains has the characteristics of compact structure, high stiffness, and high modularity. To solve the dynamic problem of the hybrid robot. Firstly, by analyzing the induced relationship between joints, the stacking robot with a local closed chain structure is transformed into two branch chain mechanisms, and the kinematic model of the robot is established using the D-H parameter method. Secondly, the Kane method is applied to model the dynamics of the two branch chains separately, and the rigid body dynamics Kane equation of the entire 4-DOF stacking robot with a closed chain structure is obtained through the augmented matrix. Finally, the SolidWorks Motion mechanical simulation platform and MATLAB software were used to program dynamic simulations and numerical calculations, and the results were compared to verify the correctness of the dynamic theory derivation. This theory provides a necessary theoretical basis for the subsequent synthesis of robot dynamic scales.

Keywords: PR1300 stacking robot; Kane equation; inverse dynamics; simulation

1. Introduction

Stacking robots are a type of industrial robot that is rapidly developing in industries such as logistics and manufacturing. With the development of automated production lines towards intelligence, efficiency, and integration, the requirements for the power performance indicators of stacking robots are also increasing [1–3]. The stacking robot with a closed chain structure has the characteristics of high stiffness, good stability, and strong load-bearing capacity [4]. At present, scholars are utilizing AI technologies such as fuzzy control and neural network control to optimize the motion control and adaptive capabilities of robots [5–7]. In addition, they have conducted extensive research on stacking robots, including configuration design and synthesis [8], kinematics calculation [9–11] and dynamic simulation [12], etc. However, there is still limited research on the dynamic theoretical model of stacking robots. The dynamics of robots are related to acceleration, load, mass, and inertia, and their characteristics include the coupling effect of each joint, the nonlinear effects of Coriolis force and centrifugal force. The main task of dynamic analysis is to analyze the relationship between driving torque and joint motion. The results of dynamic analysis are helpful for driver selection and are a prerequisite for achieving high-precision real-time control of robots. Similarly, based on dynamic analysis, structural parameters can be optimized to obtain the optimal structural

solution.

The commonly used dynamic modeling methods include: Lagrange equation [13–15], Newton Euler method [16], Kane equation [17–20], d'Alembert principle [21], and virtual work principle [22–23]. Among them, The Lagrange equation is based on the energy function and obtains the dynamic equation through differentiation. This method is relatively concise when building models, but it requires a large amount of computation when dealing with complex systems and is not easy to directly consider forces and constraints. The Newton Euler method is a method based on force balance and moment balance, suitable for both open chain and closed chain systems. This method requires gradually calculating the velocity, acceleration, and other motion parameters of each connecting rod, as well as the forces and moments between the connecting rods during the derivation process. Although the calculation process is relatively cumbersome, the physical meaning is clear, easy to understand and apply. In systems with more degrees of freedom, the computational efficiency of the Newton Euler method may be better than that of the Kane method. The D'Alembert principle is an extension of Newton's second law on a system of particles, which introduces the concept of inertial force to address dynamic problems. This method is more intuitive in establishing dynamic equations, but it also requires gradually calculating the acceleration and inertia forces of each particle, which requires a large amount of computation. The principle of virtual work is a method based on the principle of energy conservation, which solves dynamic problems by establishing the relationship between virtual displacement and virtual work. This method may have simplicity when dealing with certain specific problems, but it is not as intuitive and universal as other methods in general dynamic analysis.

However, In the inverse dynamics of closed chain stacking robots, the Kane method has certain advantages and limitations, and also has its own characteristics compared to other dynamic analysis methods.

The Kane method is suitable for multi degree of freedom discrete systems, especially for mathematical modeling of robot dynamics with closed chain structures. In the inverse dynamics of a closed chain stacking robot, the Kane method can split the closed chain into several open chains for solution, without the need to calculate the constraint forces and torque at the split points of the closed chain, thus simplifying the calculation process. The Kane method only requires step-by-step derivation from the beginning to the end of the robot to obtain the robot system model. The calculation process only involves dot product and cross product operations of vectors, and does not require differentiation operations. Compared to other methods that require complex differentiation operations, this has a smaller computational complexity. The Kane method retains the advantages of cyclic recursion in the Newton Euler method analysis process, and is formally a first-order differential equation with a standard derivation process, making it easier to implement on computers. When dealing with stacking robots with multiple closed chain structures, the Kane method can fully consider the mutual influence between local closed chains, thereby more accurately solving the real-time variation of robot driving torque.

The Kane method also has certain limitations. The concept of partial velocity in the Kane method is relatively abstract and vague, which may bring certain

difficulties in understanding and application in practical engineering applications. When the robot has fewer degrees of freedom, the total computational cost of the Kane method is lower. But as the degrees of freedom increase, the total amount of calculations in the Kane method will increase exponentially. Therefore, in systems with very high degrees of freedom, the computational efficiency of the Kane method may not be as good as other methods.

Therefore, the Kane method has broad application prospects and advantages in the inverse dynamics of closed chain stacking robots, especially in dealing with complex systems containing closed chain structures.

This article focuses on the 4-DOF PR1300 stacking robot with a closed chain structure. Because of the mutual influence between local closed chains, the Kane method is used to establish a dynamic model, and SolidWorks Motion and MATLAB software are used for dynamic simulation and verification, providing reference for future control strategy research.

2. The theoretical basis of Kane's method

2.1. Calculation of rod velocity, acceleration, and bias velocity

In order to calculate the inertial force acting on the rod, it is necessary to calculate the rotational speed, linear acceleration, and angular acceleration of each rod of the manipulator at each given moment. The relationship between velocity, acceleration, etc. in adjacent coordinate systems can be represented by a rotation transformation matrix. The recursive calculation method for the velocity, acceleration, and partial velocity of the rod and its center of mass is as follows.

Angular velocity of rod i :

$$\omega_i^i = R_{i-1}^i \cdot \omega_{i-1}^{i-1} + \dot{\theta}_i \cdot k_i^i \tag{1}$$

Linear speed of rod i :

$$v_i^i = R_{i-1}^i\left(\omega_{i-1}^{i-1} \times L_i^{i-1} + v_{i-1}^{i-1}\right) \tag{2}$$

The centroid velocity of the rod i :

$$v_{c_i}^i = v_i^i + \omega_i^i \times d_{c_i}^i \tag{3}$$

Linear acceleration of the rod i :

$$\dot{v}_i^i = R_{i-1}^i\left[\dot{v}_{i-1}^{i-1} + \dot{\omega}_{i-1}^{i-1} \times L_i^{i-1} + \omega_{i-1}^{i-1} \times \left(\omega_{i-1}^{i-1} \times L_i^{i-1}\right)\right] \tag{4}$$

Acceleration of the centroid of the rod i :

$$\dot{v}_{ci}^i = \dot{v}_i^i + \dot{\omega}_i^i \times d_{ci}^i + \omega_i^i \times \left(\omega_i^i \times d_{ci}^i\right) \tag{5}$$

The angular velocity of the rod i relative to the generalized rate $\dot{\theta}_j$:

$$\omega_{i,\dot{\theta}_j}^i = \begin{cases} R_{i-1}^i \omega_{i-1,\dot{\theta}_j}^{i-1} & j < i \\ k_i^i & j = i \\ 0 & j > i \end{cases} \tag{6}$$

The offset velocity of the rod i relative to the generalized velocity $\dot{\theta}_j$:

$$v_{i,\dot{\theta}_j}^{i} = \begin{cases} R_{i-1}^{i}(\omega_{i-1,\dot{\theta}_j}^{i-1} \times l_{i-1}^{i-1} + v_{i-1,\dot{\theta}_j}^{i-1}) & j < i \\ 0 & j \geq i \end{cases} \tag{7}$$

The offset velocity of the center of mass of the rod i relative to the generalized velocity $\dot{\theta}_j$:

$$v_{c_i,\dot{\theta}_j}^{i} = v_{i,\dot{\theta}_j}^{i} + \omega_{i,\dot{\theta}_j}^{i} \times l_{c_i}^{i} \tag{8}$$

In equations (1) to (8), L_i^{i-1} represents the distance vector from the origin of the coordinate system of rod $i-1$ to the origin of the coordinate system of rod i. d_i^i represents the distance vector from the origin of rod i coordinate system to the center of mass of rod $i-1$. R_{i-1}^{i} represents the rotation transformation matrix from the origin of rod $i-1$ coordinate system to rod i coordinate system. k_i^i represents the unit vector of the coordinate system of rod i.

2.2. Description of Kane's kinetic equation

Think of a rigid body as consisting of n particles. Let the center of mass of the rigid body be C, take the simplified center of action of C, and let the resultant force of the main force acting on the rigid body be R_C and the resultant moment be M_C.

When a rigid body rotates with an angular velocity ω, the velocity of point i is:

$$v_i = v_c + R_i \times \omega \tag{9}$$

In Equation (9), R_i is the position vector from the point to the center of mass C. v_c is the linear velocity of the center of mass C.

The partial velocity of v_i with respect to $\dot{\theta}_j$ is:

$$v_{i,\dot{\theta}_j} = \frac{\partial v_i}{\partial \dot{\theta}_j} = \frac{\partial v_c}{\partial \dot{\theta}_j} + \frac{\partial (R_i \times \omega)}{\partial \dot{\theta}_j} = v_{c,\dot{\theta}_j} + R_i \times \omega_{\dot{\theta}_j} \tag{10}$$

In the above equation, $v_{c,\dot{\theta}_j}$ represents the deflection velocity of the center of mass C with respect to $\dot{\theta}_j$, and $\omega_{\dot{\theta}_j}$ represents the deflection velocity of the rigid body with respect to $\dot{\theta}_j$.

$$v_{c,\dot{\theta}_j} = \frac{\partial v_c}{\partial \dot{\theta}_j} \tag{11}$$

$$\omega_{\dot{\theta}_j} = \frac{\partial \omega}{\partial \dot{\theta}_j} \tag{12}$$

The generalized principal force acting on rigid body with respect to the generalized rate $\dot{\theta}_j$ is:

$$\begin{aligned} F_j &= \sum_{i=1}^{n} F_i \cdot v_{i,\dot{\theta}_j} = \sum_{i=1}^{n} F_i \cdot v_{c,\dot{\theta}_j} + \sum_{i=1}^{n} F_i \cdot \left(R_i \times \omega_{\dot{\theta}_j}\right) \\ &= \sum_{i=1}^{n} F_i \cdot v_{c,\dot{\theta}_j} + \sum_{i=1}^{n} (F_i \times R_i) \cdot \omega_{\dot{\theta}_j} \\ &= R_C \cdot v_{c,\dot{\theta}_j} + M_C \cdot \omega_{\dot{\theta}_j} \end{aligned} \tag{13}$$

The generalized inertia force with respect to the generalized rate $\dot{\theta}_j$ is:

$$F_j^{'} = -\sum_{i=1}^{n} m_i a_i \cdot v_{i,\dot{\theta}_j} = -\sum_{i=1}^{n} m_i a_i \cdot v_{c,\dot{\theta}_j} - \sum_{i=1}^{n} F_i \cdot (m_i a_i \times R_i)\, \omega_{\dot{\theta}_j} \tag{14}$$

Because of

$$\sum_{i=1}^{n} (m_i a_i \times R_i) = \frac{d}{dt}\left(\sum_{i=1}^{n} (m_i v_i \times R_i)\right) = \frac{dH_c}{dt} \tag{15}$$

In Equation (15), the moment of momentum H_c is expressed as the inertia tensor of a rigid body.

$$\begin{bmatrix} H_x \\ H_y \\ H_z \end{bmatrix} = \begin{bmatrix} I_{xx} & -I_{xy} & I_{xz} \\ -I_{yx} & I_{yy} & I_{yz} \\ -I_{zx} & -I_{zy} & I_{zz} \end{bmatrix} \begin{bmatrix} \omega_x \\ \omega_y \\ \omega_z \end{bmatrix} \tag{16}$$

So, if we take the time derivative of H_c, we get:

$$\frac{dH_c}{dt} = \sum_{i=1}^{n} (m_i a_i \times R_i) = I\dot{\omega} + \omega \times I\omega \tag{17}$$

So, the generalized inertial force can be expressed as:

$$F_j^{'} = -\sum_{i=1}^{n} m_i a_i \cdot v_{c,\dot{\theta}_j} - (I\dot{\omega} + \omega \times I\omega) \cdot \omega_{\dot{\theta}_j} (j = 1,2,\cdots l) \tag{18}$$

By adding Equations (14) and (19), Kane's dynamic equation for a rigid body is:

$$R_C \cdot v_{C,\dot{\theta}_j} + M_C \cdot \omega_{\dot{\theta}_j} = \sum_{i=1}^{n} m_i a_i \cdot v_{c,\dot{\theta}_j} + N_C \cdot \omega_{\dot{\theta}_j}\, (j = 1,2,\cdots, l) \tag{19}$$

Equation (19) is Kane's dynamic equation for a rigid body, which means that the generalized principal force and generalized inertia force corresponding to the generalized rate of the system are equal. Where, $N_C = I\dot{\omega} + \omega \times I\omega$; Irepresents the inertia tensor of a rigid body with respect to the center of mass C.

For a robot system with multiple rigid bodies, Kane's dynamic equation is used and the partial velocity is substituted into the formula, and the formula for calculating the joint driving torque can be obtained as follows:

$$\tau_{\dot{\theta}_j} = \sum_{i=j}^{n} M_{i\dot{\theta}_j} = \sum_{i=j}^{n} m_i \dot{v}_{c_i}^i \cdot v_{c_i\theta_j}^i + \sum_{i=j}^{n} N_i \, \omega_{i\theta_j}^i - \sum_{i=j}^{n} R_{c_i}^i \, v_{c_i\theta_j}^i - \sum_{i=j}^{n} M_{c_i}^i \, \omega_{i\theta_j}^i \quad (20)$$

3. Inverse dynamics analysis of PR1300 stacking robot

3.1. Generalized system speed

There are two common types of 4-DOF local closed-chain stacking robots, one is the coaxial arrangement of 2-axis and 3-axis motors [24], and the other is the vertical arrangement of 2-axis and 3-axis motors [25], both of which are widely used in industry. The 2-axis and 3-axis motors of the PR1300 stacking robot are arranged in a coaxial manner.

Figure 1 is A schematic diagram of the PR1300 stacking robot mechanism. Joint θ_4 is constrained by locally closed chains II and III so that the end effector is always level. If the forearm drive link, horizontal triangle arm and horizontal holding link are ignored, θ_4 is regarded as the active joint, the original four-degree-of-freedom local closed-chain stacking robot is transformed into five degree-of-freedom robot , joint $\theta_1, \theta_2, \theta_{2'}, \theta_4, \theta_5$is the active joint variable, and joint$\theta_3, \theta_{3'}, \theta_{4'}$ is the slave joint variable.

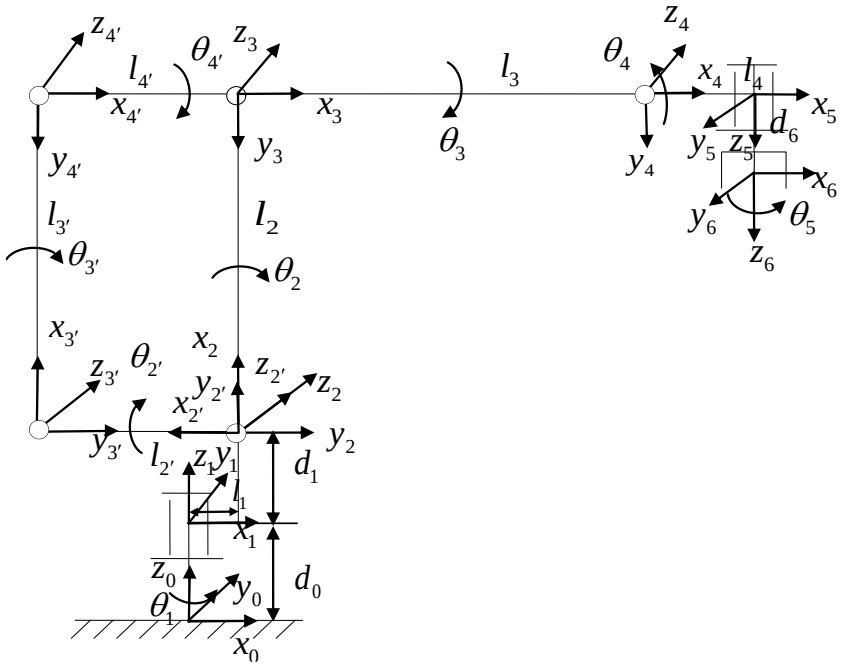

Figure 1. PR1300 stacking robot mechanism schematic.

According to the motion characteristics of the mechanism, the model is simplified without affecting the accuracy of the robot dynamics modeling. Ignoring active joint variables θ_4 and θ_5, the end wrist bracket is directly fixed at the end of rod l_3 , and active joint $\theta_1, \theta_2, \theta_{2'}$ are selected as the independent generalized coordinate of the system, and $\dot{\theta}_1, \dot{\theta}_2, \dot{\theta}_{2'}$ are the generalized rate of the system. In order to determine the relationship between the generalized rate of the system and

other non-generalized rates, the closed chain structure of the stacking robot is divided into two ways, left and right, as shown in **Figure 2**.

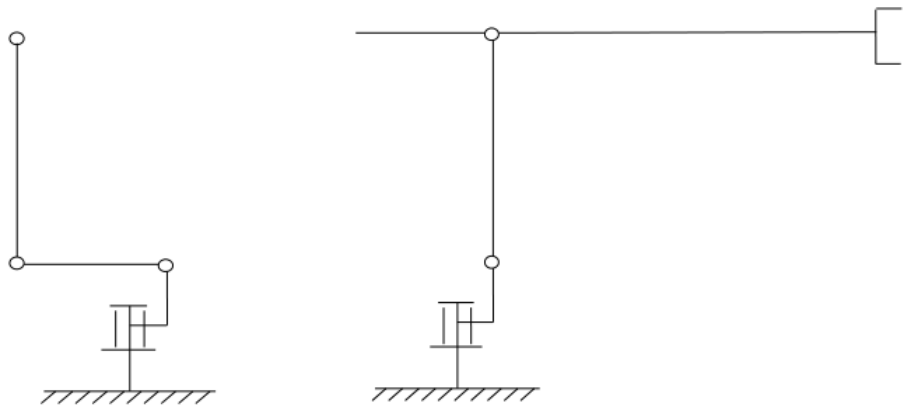

Figure 2. Equivalent chain opening diagram of stacking robot.

The structure parameters and motion parameters of the simplified 4-DOF local closed chain stacking robot is shown in **Table 1**.

Table 1. Structural parameters and motion parameters.

Rod i	α (°)	a (mm)	d (mm)	θ (°)	θ_0 (°)
l_1	0	0	d_0	θ_1	0
l_2	−90	l_1	d_1	θ_2	−90
l_3	0	l_2	0	θ_3	90
$l_{2'}$	−90	l_1	d_1	θ_2	−180
$l_{3'}$	0	$l_{2'}$	0	$\theta_{3'}$	90
$l_{4'}$	0	$l_{3'}$	0	$\theta_{4'}$	90
l_4	0	l_3	0	θ_4	0

Forward kinematic analysis of left and right open chains are carried out respectively.

3.1.1. For the right open chain

In Equation (21), T_{i+1}^{i} represents the translation transformation matrix from the origin of the rod $i+1$ coordinate system to the rod i coordinate system, $s_1 = \sin\theta_1, c_1 = \cos\theta_1, s_{2+3} = \sin(\theta_2+\theta_3), c_{2+3} = \cos(\theta_2+\theta_3)$.

$$T_1^0 = \begin{bmatrix} c_1 & -s_1 & 0 & 0 \\ s_1 & c_1 & 0 & d_0 \\ 0 & 0 & 1 & 0 \\ 0 & 0 & 0 & 1 \end{bmatrix} \quad R_1^0 = \begin{bmatrix} c_1 & -s_1 & 0 \\ s_1 & c_1 & 0 \\ 0 & 0 & 1 \end{bmatrix}$$

$$T_2^1 = \begin{bmatrix} s_2 & c_2 & 0 & l_1 \\ 0 & 0 & 1 & d_1 \\ c_2 & -s_2 & 0 & 0 \\ 0 & 0 & 0 & 1 \end{bmatrix} \quad R_2^1 = \begin{bmatrix} s_2 & c_2 & 0 \\ 0 & 0 & 1 \\ c_2 & -s_2 & 0 \end{bmatrix}$$

$$T_3^2 = \begin{bmatrix} -s_3 & -c_3 & 0 & l_2 \\ c_3 & -s_3 & 0 & 0 \\ 0 & 0 & 1 & 0 \\ 0 & 0 & 0 & 1 \end{bmatrix} \quad R_3^2 = \begin{bmatrix} -s_3 & -c_3 & 0 \\ c_3 & -s_3 & 0 \\ 0 & 0 & 1 \end{bmatrix}$$

$$\begin{aligned} RT_3^0 &= T_1^0 T_2^1 T_3^2 \\ &= \begin{bmatrix} c_1c_{2+3} & -c_1c_{2+3} & -s_1 & c_1s_2l_2 + c_1l_1 - s_1d_1 \\ s_1c_{2+3} & -s_1c_{2+3} & c_1 & s_1s_2l_2 + s_1l_1 + c_1d_1 + d_0 \\ -s_{2+3} & -c_{2+3} & 0 & c_2l_2 \\ 0 & 0 & 0 & 1 \end{bmatrix} \end{aligned} \tag{21}$$

3.1.2. For the left open chain

$$T_{2'}^1 = \begin{bmatrix} -c_{2'} & s_{2'} & 0 & l_1 \\ 0 & 0 & 1 & d_1 \\ s_{2'} & c_{2'} & 0 & 0 \\ 0 & 0 & 0 & 1 \end{bmatrix} \quad R_{2'}^1 = \begin{bmatrix} -c_{2'} & s_{2'} & 0 \\ 0 & 0 & 1 \\ s_{2'} & c_{2'} & 0 \end{bmatrix}$$

$$T_{3'}^{2'} = \begin{bmatrix} -s_{3'} & -c_{3'} & 0 & l_{2'} \\ c_{3'} & -s_{3'} & 0 & 0 \\ 0 & 0 & 1 & 0 \\ 0 & 0 & 0 & 1 \end{bmatrix} \quad R_{3'}^{2'} = \begin{bmatrix} -s_{3'} & -c_{3'} & 0 \\ c_{3'} & -s_{3'} & 0 \\ 0 & 0 & 1 \end{bmatrix}$$

$$T_{4'}^{3'} = \begin{bmatrix} -s_{4'} & -c_{4'} & 0 & l_{3'} \\ c_{4'} & -s_{4'} & 0 & 0 \\ 0 & 0 & 1 & 0 \\ 0 & 0 & 0 & 1 \end{bmatrix} \quad R_{4'}^{3'} = \begin{bmatrix} -s_{4'} & -c_{4'} & 0 \\ c_{4'} & -s_{4'} & 0 \\ 0 & 0 & 1 \end{bmatrix}$$

$$T_3^{4'} = \begin{bmatrix} 1 & 0 & 0 & l_{4'} \\ 0 & 1 & 0 & 0 \\ 0 & 0 & 1 & 0 \\ 0 & 0 & 0 & 1 \end{bmatrix} \quad R_3^{4'} = \begin{bmatrix} 1 & 0 & 0 \\ 0 & 1 & 0 \\ 0 & 0 & 1 \end{bmatrix}$$

$$\begin{aligned} LT_3^0 &= T_1^0 T_{2'}^1 T_{3'}^{2'} T_{4'}^{3'} T_3^{4'} \\ &= \begin{bmatrix} c_1c_{2'+3'+4'} & -c_1s_{2'+3'+4'} & -s_1 & c_1c_{2'+3'+4'}l_{4'} + c_1s_{2'+3'}l_{3'} - c_1c_{2'}l_{2'} + c_1l_1 - s_1d_1 \\ s_1c_{2'+3'+4'} & -s_1s_{2'+3'+4'} & c_1 & s_1c_{2'+3'+4'}l_{4'} + s_1s_{2'+3'}l_{3'} - s_1c_{2'}l_{2'} + s_1l_1 + c_1d_1 + d_0 \\ -s_{2'+3'+4'} & -c_{2'+3'+4'} & 0 & -s_{2'+3'+4'}l_{4'} + c_{2'+3'}l_{3'} + s_{2'}l_{2'} \\ 0 & 0 & 0 & 1 \end{bmatrix} \end{aligned} \tag{22}$$

In Equation (22), $s_1 = \sin\theta_1, c_1 = \cos\theta_1, s_{2'+3'+4'} = \sin(\theta_{2'} + \theta_{3'} + \theta_{4'}), c_{2'+3'+4'} = \cos(\theta_{2'} + \theta_{3'} + \theta_{4'})$.

Through forward kinematic analysis of the left and right open chains, the position and pose of the end effector should be the same, that is, $RT_3^0 = LT_3^0$. It is also known from the structure conditions of PR1300 stacking robot, $l_2 = l_{3'}, l_{2'} = l_{4'}$ and $\theta_{4'} = \theta_3$, so the relationship between the independent generalized coordinates of the system and other non-independent generalized coordinates can be easily obtained as follows:

$$\begin{cases} \theta_{3'} = \theta_2 - \theta_{2'} \\ \theta_{4'} = \theta_3 = \theta_{2'} - \theta_2 \end{cases} \tag{23}$$

After differentiating both ends, the relationship between the generalized rate and other non-generalized rates of the system is

$$\begin{cases} \dot{\theta}_{3'} = \dot{\theta}_2 - \dot{\theta}_{2'} \\ \dot{\theta}_{4'} = \dot{\theta}_3 = \dot{\theta}_{2'} - \dot{\theta}_2 \end{cases} \tag{24}$$

3.2. Solving the driving torque of the active joint

According to Equations (1)–(20), the driving torque of each arm rod in the left and right open chain is calculated respectively. Considering the gravity of the robot rod, $\dot{v}_0^0 = [0 \quad 0 \quad g]^T$ is taken as the initial value, $\omega_0^0, \dot{\omega}_0^0$ and v_0^0 are taken as $[0 \quad 0 \quad 0]^T$.

3.2.1. Find the driving torque on the left open chain

The driving torque $M_{i\dot{\theta}_j}$ $(i = 1, 2', 3'; j = 1, 2, 2')$ can be obtained for the $l_1, l_{2'}, l_{3'}$ rods in the left open chain.

For bar l_1, the angular velocity is:

$$\omega_1^1 = R_0^1 \omega_0^0 + \dot{\theta}_1 k_1^1 = \begin{bmatrix} 0 \\ 0 \\ \dot{\theta}_1 \end{bmatrix} \tag{25}$$

Deflection velocity with respect to generalized velocity $\dot{\theta}_j$:

$$\omega_{1\dot{\theta}_1}^1 = \begin{bmatrix} 0 \\ 0 \\ 1 \end{bmatrix}, \omega_{1\dot{\theta}_2}^1 = \begin{bmatrix} 0 \\ 0 \\ 0 \end{bmatrix}, \omega_{1\dot{\theta}_{2'}}^1 = \begin{bmatrix} 0 \\ 0 \\ 0 \end{bmatrix} \tag{26}$$

Linear velocity:

$$v_1^1 = R_0^1(\omega_0^0 \times L_1^0 + v_0^0) = \begin{bmatrix} 0 \\ 0 \\ 0 \end{bmatrix} \tag{27}$$

Linear velocity of center of mass:

$$v_{1c_1}^1 = v_1^1 + \omega_1^1 \times d_{1c}^1 = \begin{bmatrix} 0 \\ d_{1c}^1 \dot{\theta}_1 \\ 0 \end{bmatrix} \tag{28}$$

The deflection velocity of the center of mass with respect to $\dot{\theta}_j$:

$$v_{1c\dot{\theta}_1}^1 = \begin{bmatrix} 0 \\ d_{c_1}^1 \\ 0 \end{bmatrix}, v_{1c\dot{\theta}_2}^1 = \begin{bmatrix} 0 \\ 0 \\ 0 \end{bmatrix}, v_{1c\dot{\theta}_{2'}}^1 = \begin{bmatrix} 0 \\ 0 \\ 0 \end{bmatrix} \tag{29}$$

Angular acceleration:

$$\dot{\omega}_1^1 = R_0^1 \dot{\omega}_0^0 + R_0^1 \omega_0^0 \times \dot{\theta}_1 k_1^1 + \ddot{\theta}_1 k_1^1 = \begin{bmatrix} 0 \\ 0 \\ \ddot{\theta}_1 \end{bmatrix} \tag{30}$$

Linear acceleration:

$$\dot{v}_1^1 = R_0^1[\dot{v}_0^0 + \dot{\omega}_0^0 \times L_0^0 + \omega_0^0 \times (\omega_0^0 \times L_0^0)] = \begin{bmatrix} 0 \\ 0 \\ g \end{bmatrix} \tag{31}$$

Line acceleration of the center of mass:

$$\dot{v}_{1c}^1 = \dot{v}_1^1 + \dot{\omega}_1^1 \times d_{c_1}^1 + \omega_1^1 \times (\omega_1^1 \times d_{1c}) = \begin{bmatrix} -d_{1c}^1(\dot{\theta}_1)^2 \\ g d_{1c}^1 \\ 0 \end{bmatrix} \tag{32}$$

Inertia moment:

$$N_1^1 = I_{1zz}\dot{\omega}_1^1 + \omega_1^1 \times I_{1zz}\omega_1^1 = \begin{bmatrix} 0 \\ 0 \\ I_{1zz}\ddot{\theta}_1 \end{bmatrix} \tag{33}$$

Joint driving torque:

$$M_{1\dot{\theta}_1} = m_1 \cdot \dot{v}_{1c}^1 \cdot v_{1c\dot{\theta}_1}^1 + N_1^1 \cdot \omega_{1\dot{\theta}_1}^1 = m_1 g (d_{1c}^1)^2 + I_{1zz}\ddot{\theta}_1$$

$$M_{1\dot{\theta}_2} = m_1 \cdot \dot{v}_{1c}^1 \cdot v_{1c\dot{\theta}_1}^1 + N_1^1 \cdot \omega_{1\dot{\theta}_1}^1 = 0 \tag{34}$$

$$M_{1\dot{\theta}_{2'}} = m_1 \cdot \dot{v}_{1c}^1 \cdot v_{1c\dot{\theta}_{2'}}^1 + N_1^1 \cdot \omega_{1\dot{\theta}_{2'}}^1 = 0$$

For bar $l_{2'}$, the whole calculation process is similar to bar l_1, and the calculation result is given directly.

$$\begin{aligned} M_{2'\dot{\theta}_1} &= m_{2'} \cdot \dot{v}_{2'c}^{2'} \cdot v_{2'c\dot{\theta}_1}^{2'} + N_{2'}^{2'}\omega_{2'\dot{\theta}_1}^{2'} \\ &= m_{2'}(l_1 - d_{2'c}^{2'}c_{2'})(2d_{2'c}^{2'}s_{2'}\dot{\theta}_1\dot{\theta}_{2'} + l_1\ddot{\theta}_1 - d_{2'c}^{2'}c_{2'}\ddot{\theta}_1) \end{aligned}$$

$$M_{2'\dot{\theta}_2} = m_{2'} \cdot \dot{v}_{2'c}^{2'} \cdot v_{2'c\dot{\theta}_2}^{2'} + N_{2'}^{2'}\omega_{2'\dot{\theta}_2}^{2'} = 0 \tag{35}$$

$$\begin{aligned} M_{2'\dot{\theta}_{2'}} &= m_{2'} \cdot \dot{v}_{2'c}^{2'} \cdot v_{2'c\dot{\theta}_{2'}}^{2'} + N_{2'}^{2'}\omega_{2'\dot{\theta}_{2'}}^{2'} \\ &= m_{2'} \cdot d_{2'c}^{2'}[c_{2'}g - l_1 s_{2'}(\dot{\theta}_1)^2 + d_{2'c}^{2'}\ddot{\theta}_{2'} + s_{2'}c_{2'}(\dot{\theta}_1)^2] + I_{2'zz}\ddot{\theta}_{2'}\sqrt{b^2 - 4ac} \end{aligned}$$

For bar $l_{3'}$, the whole calculation process is similar to bar l_1, and the calculation result is given directly.

$$\begin{aligned} M_{3'\dot{\theta}_1} &= m_{3'}\dot{v}_{3'c}^{3'}v_{3'c\dot{\theta}_1}^{3'} + N_{3'}^{3'}\omega_{3'\dot{\theta}_1}^{3'} \\ &= m_{3'} \cdot (l_1 - l_{2'}c_{2'} + d_{3'c}^{3'}s_2)[l_1\ddot{\theta}_1 + 2l_{2'}s_{2'}\theta_1\theta_{2'} - l_{2'}c_{2'}\ddot{\theta}_1 + 2d_{3'c}^{3'}c_2\dot{\theta}_1\dot{\theta}_2 + d_{3'c}^{3'}s_2\ddot{\theta}_1 + d_{3'c}^{3'}c_2\dot{\theta}_1\dot{\theta}_{2-2'}] \end{aligned}$$

$$\begin{aligned} M_{3'\dot{\theta}_2} &= m_{3'}\dot{v}_{3'c}^{3'}v_{3'c\dot{\theta}_2}^{3'} + N_{3'}^{3'}\omega_{3'\dot{\theta}_2}^{3'} \\ &= m_{3'} \cdot d_{3'c}^{3'} \cdot [-l_1 c_2(\dot{\theta}_1)^2 + l_{2'}c_{2'}c_2(\dot{\theta}_1)^2 + l_{2'}c_{2-2'}(\dot{\theta}_{2'})^2 - l_{2'}s_{2-2'}\ddot{\theta}_{2'} \\ &\quad -s_2 g + d_{3'c}^{3'}(\ddot{\theta}_{2'} + \ddot{\theta}_{3'}) - d_{3'c}^{3'}s_2 c_2(\dot{\theta}_1)^2] + I_{3'zz}(\ddot{\theta}_{2'} + \ddot{\theta}_{3'}) \end{aligned} \tag{36}$$

$$\begin{aligned} M_{3'\dot{\theta}_{2'}} &= m_{3'}\dot{v}_{3'c}^{3'}v_{3'c\dot{\theta}_{2'}}^{3'} + N_{3'}^{3'}\omega_{3'\dot{\theta}_{2'}}^{3'} \\ &= m_{3'}[l_1 l_{2'}s_{2'}(\dot{\theta}_1)^2 + s_{2'}c_{2'}(l_{2'}\dot{\theta}_1)^2 + (l_{2'})^2\ddot{\theta}_{2'} + l_{2'}c_{2'}g - d_{3'c}^{3'}l_{2'}c_{2-2'}(s_2\dot{\theta}_1)^2 \\ &\quad -d_{3'c}^{3'}l_{2'}c_{2-2'}(\dot{\theta}_2)^2 - l_{2'}d_{3'c}^{3'}s_{2-2'}(\ddot{\theta}_{2'} + \ddot{\theta}_{3'}) + l_{2'}d_{3'c}^{3'}s_{2-2'}s_2 c_2(\dot{\theta}_1)^2] \end{aligned}$$

3.2.2. Right open chain to find the driving torque

Similarly, the driving torque $M_{i\dot{\theta}_j}(i=2,3;j=1,2,2')$ can be obtained for rod l_2, l_3in the right open chain

For the l_2 bar, we can find

$$\begin{aligned} M_{2\dot{\theta}_1} &= m_2 \cdot \dot{v}_{2c}^2 \cdot v_{2c\dot{\theta}_1}^2 + N_2^2 \omega_{2\dot{\theta}_1}^2 \\ &= -m_2(l_1 + d_{2c}^2 s_2)(l_1\ddot{\theta}_1 + 2d_{2c}^2 c_2 \dot{\theta}_1\dot{\theta}_2 + d_{2c}^2 s_2\ddot{\theta}_1) \end{aligned} \tag{37}$$

$$\begin{aligned} M_{2\dot{\theta}_2} &= m_2 \cdot \dot{v}_{2c}^2 \cdot v_{2c\dot{\theta}_2}^2 + N_2^2 \omega_{2\dot{\theta}_2}^2 \\ &= m_2 d_{2c}^2[-l_1 c_2(\dot{\theta}_1)^2 - s_2 g + d_{2c}^2\ddot{\theta}_2 - d_{2c}^2 s_2 c_2(\dot{\theta}_1)^2] + I_{2zz}\ddot{\theta}_2 \end{aligned}$$

$$M_{2\dot{\theta}_{2'}} = m_2 \cdot \dot{v}_{2c}^2 \cdot v_{2c\dot{\theta}_{2'}}^2 + N_2^2 \omega_{2\dot{\theta}_{2'}}^2 = 0$$

For the l_3 bar, we can find

$$\begin{aligned} M_{3\dot{\theta}_1} &= m_3 \dot{v}_{3c}^3 v_{3c\dot{\theta}_1}^3 + N_3^3 \omega_{3\dot{\theta}_1}^3 \\ &= m_3(l_1 + l_2 s_2 + d_{3c}^3 s_{2'})[l_1\ddot{\theta}_1 + 2l_2 c_2\dot{\theta}_1\dot{\theta}_2 + l_2 s_2\ddot{\theta}_1 - d_{3c}^3(s_{2'}\dot{\theta}_1\dot{\theta}_2 - c_{2'}\ddot{\theta}_1 + s_{2'}\dot{\theta}_1\dot{\theta}_{2'-2}) - d_{3c}^3 s_{2'}\dot{\theta}_1\dot{\theta}_{2'}] \end{aligned}$$

$$\begin{aligned} M_{3\dot{\theta}_2} &= m_3 \dot{v}_{3c}^3 v_{3c\dot{\theta}_2}^3 + N_3^3 \omega_{3\dot{\theta}_2}^3 \\ &= m_3[-l_1 l_2 c_2(\dot{\theta}_1)^2 - s_2 c_2(l_2\dot{\theta}_1)^2 + (l_2)^2\ddot{\theta}_2 - l_2 s_2 g - l_2 d_{3c}^3 c_{2'-2}(c_{2'}\dot{\theta}_1)^2 \\ &\quad -l_2 d_{3c}^3 c_{2'-2}(\dot{\theta}_{2'})^2 - l_2 d_{3c}^3 s_{2'-2}(\ddot{\theta}_2 + \ddot{\theta}_3) + l_2 d_{3c}^3 s_{2'} c_{2'} s_{2'-2}(\dot{\theta}_1)^2] \end{aligned} \tag{38}$$

$$\begin{aligned} M_{3\dot{\theta}_{2'}} &= m_3 \dot{v}_{3c}^3 v_{3c\dot{\theta}_{2'}}^3 + N_3^3 \omega_{3\dot{\theta}_{2'}}^3 \\ &= m_3 d_{3c}^3[l_1 s_{2'}(\dot{\theta}_1)^2 + l_2 s_2 s_{2'}(\dot{\theta}_1)^2 + l_2 c_{2'-2}(\dot{\theta}_2)^2 - l_2 s_{2'-2}\ddot{\theta}_2 - c_{2'} g \\ &\quad + d_{3c}^3(\ddot{\theta}_2 + \ddot{\theta}_3) - d_{3c}^3 s_{2'} c_{2'}(\dot{\theta}_1)^2] + I_{3zz}(\ddot{\theta}_2 + \ddot{\theta}_3) \end{aligned}$$

Let $\tau_i(i=1,2,2')$ represent the driving torque of joint i, and get the system inverse dynamic equation of rigid body:

$$\tau_i = \sum_{i=j} M_{i\dot{\theta}_j} = \tau_{g_i} + \tau_{a_i} + \tau_{v_i}\left(j = 1,2,2',3,3',4\right) \tag{39}$$

In Equation (25), τ_{g_i}, τ_{a_i} and τ_{v_i} respectively represent the gravity term, inertia term and velocity term in the joint driving torque. Among them,

$$\tau_{g_i} = \begin{bmatrix} \tau_{g_1} \\ \tau_{g_2} \\ \tau_{g_{2'}} \end{bmatrix} = \begin{bmatrix} m_1(d_{1c}^1)^2 g \\ -(m_{3'} d_{3'c}^{3'} s_2 + m_2 d_{2c}^2 s_2 + m_3 l_2 s_2) g \\ (m_{2'} \cdot d_{2'c}^{2'} c_{2'} + m_{3'} l_{2'} c_{2'} - m_3 d_{3c}^3 c_{2'}) g \end{bmatrix}$$

$$\tau_{a_i} = \begin{bmatrix} \tau_{a_1} \\ \tau_{a_2} \\ \tau_{a_{2'}} \end{bmatrix} = \begin{bmatrix} m_{2'}(l_1 - d_{2'c}^{2'} c_{2'})^2\ddot{\theta}_1 + m_{3'} \cdot (l_1 - l_{2'} c_{2'} + d_{3'c}^{3'} s_2)^2\ddot{\theta}_1 + m_3(l_1 + l_2 s_2 + d_{3c}^3 s_{2'})^2\ddot{\theta}_1 \\ -m_2(l_1 + d_{2c}^2 s_2)^2\ddot{\theta}_1 + I_{1zz}\ddot{\theta}_1 \\ [m_{3'} \cdot (d_{3'c}^{3'})^2 + m_2(d_{2c}^2)^2 + m_3(l_2)^2]\ddot{\theta}_2 - (m_3 l_2 d_{3c}^3 s_{2'-2} + m_{3'} \cdot l_{2'} d_{3'c}^{3'} s_{2-2'})\ddot{\theta}_{2'} \\ +(I_{3'zz} + I_{2zz})\ddot{\theta}_2 \\ [m_3(d_{3c}^3)^2 + m_{2'} \cdot (d_{2'c}^{2'})^2 + m_{3'}(l_{2'})^2]\ddot{\theta}_{2'} - (m_{3'} l_{2'} d_{3'c}^{3'} s_{2-2'} + m_3 d_{3c}^3 l_2 s_{2'-2})\ddot{\theta}_2 \\ +(I_{2'zz} + I_{3zz})\ddot{\theta}_{2'} \end{bmatrix} \tag{40}$$

$$\tau_{v_i}=\begin{bmatrix}\tau_{v_1}\\ \tau_{v_2}\\ \tau_{v_{2'}}\end{bmatrix}=\begin{bmatrix}2m_{2'}d_{2'c}^{2'}s_{2'}(l_1-d_{2'c}^{2'}c_{2'})\dot{\theta}_{2'}\dot{\theta}_1+m_{3'}\cdot(l_1-l_{2'}c_{2'}+d_{3'c}^{3'}s_2)[2l_{2'}s_{2'}\theta_{2'}+2d_{3'c}^{3'}c_2\dot{\theta}_2\\ +d_{3'c}^{3'}c_2\dot{\theta}_{2-2'}]\dot{\theta}_1-2m_2d_{2c}^2c_2(l_1+d_{2c}^2s_2)\dot{\theta}_2\dot{\theta}_1+m_3(l_1+l_2s_2+d_{3c}^3s_{2'})[2l_2c_2\dot{\theta}_2-\\ d_{3c}^3(s_{2'}\dot{\theta}_2+s_{2'}\dot{\theta}_{2'-2})-d_{3c}^3s_{2'}\dot{\theta}_{2'}]\dot{\theta}_1\\ m_{3'}\cdot d_{3'c}^{3'}\cdot[-l_1c_2+l_{2'}c_{2'}c_2-d_{3'c}^{3'}s_2c_2](\dot{\theta}_1)^2+m_2d_{2c}^2[-l_1c_2-d_{2c}^2s_2c_2](\dot{\theta}_1)^2\\ m_3[-l_1l_2c_2-(l_2)^2s_2c_2-l_2d_{3c}^3(c_{2'})^2c_{2'-2}+l_2d_{3c}^3s_{2'}c_{2'}s_{2'-2}](\dot{\theta}_1)^2-m_3l_2d_{3c}^3c_{2'-2}\\ (\dot{\theta}_{2'})^2+m_{3'}\cdot d_{3'c}^{3'}l_{2'}c_{2-2'}(\dot{\theta}_{2'})^2\\ m_{2'}\cdot d_{2'c}^{2'}(s_{2'}c_{2'}-l_1s_{2'})(\dot{\theta}_1)^2+m_{3'}[l_1l_{2'}s_{2'}+s_{2'}c_{2'}(l_{2'})^2-d_{3'c}^{3'}l_{2'}c_{2-2'}(s_2)^2\\ +l_{2'}d_{3'c}^{3'}s_{2-2'}s_2c_2](\dot{\theta}_1)^2+m_3d_{3c}^3[l_1s_{2'}+l_2s_2s_{2'}-d_{3c}^3s_{2'}c_{2'}](\dot{\theta}_1)^2+(m_3d_{3c}^3l_2c_{2'-2}\\ -m_{3'}d_{3'c}^{3'}l_{2'}c_{2-2'})(\dot{\theta}_2)^2\end{bmatrix}$$

4. Dynamic simulation

In order to verify the correctness of dynamic calculation based on KANE method, MATLAB was used for dynamic simulation based on the above theoretical derivation. At the same time, SolidWorks software is used to establish the three-dimensional model of the stacking robot, set the material properties, and carry out the dynamic simulation of the driving torque of the upper and lower arm joints with SolidWorks Motion. Based on the same trajectory planning data, the correctness of dynamic derivation based on KANE method in this paper is verified by comparing the simulation results of the two methods. The verification route of kinetic theory derivation is shown in **Figure 3**.

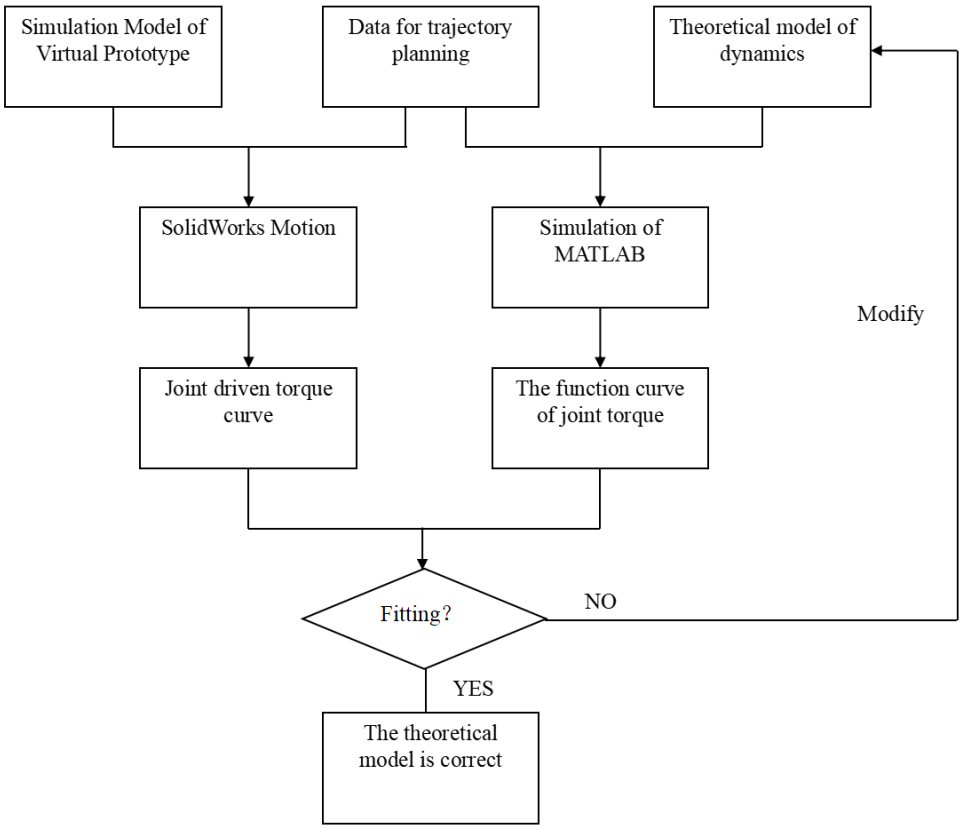

Figure 3. Verification route of kinetic theory derivation.

4.1. Virtual prototype model of stacking robot based on solid works

SolidWorks is a full three-dimensional parametric mechanical design platform integrating CAD/CAE/CAM launched by Dassault Systems, a French company. SolidWorks is one of the most widely used computer aided design, analysis and manufacturing software in the field of mechanical engineering in the world. It provides a powerful feature-based parametric solid modeling function, users can stretch, rotate, scan, lofting and other different feature tools for product design.

For assembly design, SolidWorks provides intelligent constraint assembly technology that automatically reasoning and provides fit options for the designer, as well as dynamic interference inspection and clearance detection of moving parts.

In this paper, SolidWorks software is used to model the main parts of PR1300 stacking robot. On the basis of this, the virtual prototype model of PR1300 stacking robot is established through the assembly form of SolidWorks software.

The main structural scale parameters of PR1300 stacking robot are shown in **Table 2**:

Table 2. Parameters of the main parts and dimensions of the stacking robot (unit: mm).

Component Name	Dimensional parameters (length * cross-sectional size)	Material
Big arm	1220 × 25 × 25	HT200
Forearm	1300 × 18 × 18	HT200
Drive arm of forearm	590 × 70 × 130	HT200
Drive linkage of forearm	1220 × 186 × 51	HT200
Horizontal holding 1 link	1220 × 60 × 40	HT200
Horizontal holding 1 link	1300 × 60 × 40	HT200

The selection of each joint servo motor and reducer is shown in **Table 3**:

Table 3. Parameters of each joint motor and reducer.

Joint	Electrical machinery	Reducer
Base joint	Model: Siemens 1FT7102-5AF7 Rated power: 6280 w Rated speed: 3000 r/min Moment of inertia: 63.6×10^{-4} kg · m^2	RV-400C Speed ratio: 209 Output torque: 3752 N · m
The joints of the big arm	Model: Siemens 1FT7086-1AF7 Rated power: 5650 w Rated speed: 3000 r/min Moment of inertia 63.6×10^{-4} kg · m^2	RV-450E Speed ratio: 192 Output torque: 4410 N · m
The joints of the forearm	Model: Siemens 1FT7086-1AF7 Rated power: 5650 w Rated speed: 3000 r/min Moment of inertia 63.6×10^{-4} kg · m^2	RV-320E Speed ratio: 189 Output torque: 3136 N · m
Wrist joint	Model: Siemens 1FT7064-1AF7 Rated power: 2390 w Rated speed: 3000 r/min Moment of inertia 11.9×10^{-4} kg · m^2	RV-80E Speed ratio: 121 Output torque: 784 N · m

A virtual prototype model of PR1300 stacking robot was established

considering the appearance, weight, rigidity and machining difficulty of parts.

4.2. Dynamic simulation of stacking robot based on Solidworks motion

Solidworks Motion is a powerful 3D kinematics and dynamics simulation plug-in from SolidWorks that simulates the mechanical actions of assemblies and their resulting forces, driving torques, displacements, and velocities. It provides a variety of motion motor, spring, force and damping options to simulate the real environment, enabling users to simulate various mechanical structures, accurately predict load changes, and calculate the change curve of speed, acceleration and driving torque. Therefore, this chapter decides to use Solidworks Motion as the dynamic simulation platform of PR1300 stacking robot.

The motion path of the robot end effector is set as a straight-line segment between two path points p1 = [1800 0 800] and p2 = [1800 0 1500]. In the dynamic simulation, the modified trapezoid was selected as the robot acceleration motion law, and the maximum acceleration during the robot motion was set as 3200 mm/s^2: The maximum speed is 1200 mm/s. Under the Motion law determined by the trajectory planning, the displacement data points of each joint with a time interval of 0.01s on the movement path of the PR1300 palletiste robot are saved into txt format files according to the data format required by SolidWorks Motion.

In order to reduce the complexity of simulation calculation, some unimportant parts were deleted without affecting the overall assembly relationship of the robot, and the existence of friction was ignored in the simulation process, and the simulation model of SolidWorks Motion was obtained, as shown in **Figure 4**.

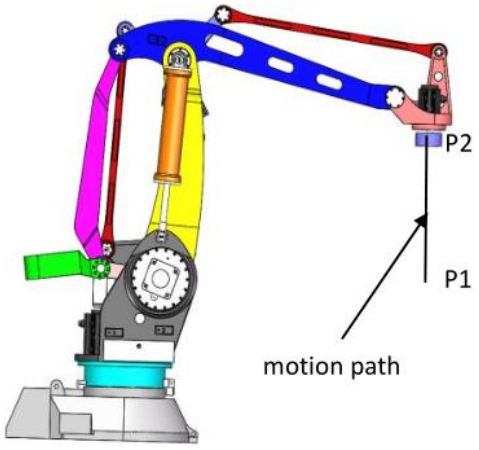

Figure 4. Schematic of the motion path of the stacking robot.

In SolidWorks, a rotating motor was added to each joint of the robot virtual prototype model, the gravity parameter was set as 9800 mm/s^2, the motor movement mode was selected to import data points into the mode, the txt file of the obtained displacement data points was imported, and the interpolation type was selected cubic spline curve.

4.3. Comparison of simulation results based on SolidWorks motion and MATLAB

The displacement, velocity and acceleration values of each joint of PR1300

stacking robot with a time interval of 0.01s on the moving path were obtained from the trajectory planning, which were substituted into the dynamic theory model, and the function curve of the robot joint torque was fitted. As shown in **Figure 5**, in order to compare the simulation results of driving torque of the upper and lower arm joints based on SolidWorks Motion and MATLAB respectively.

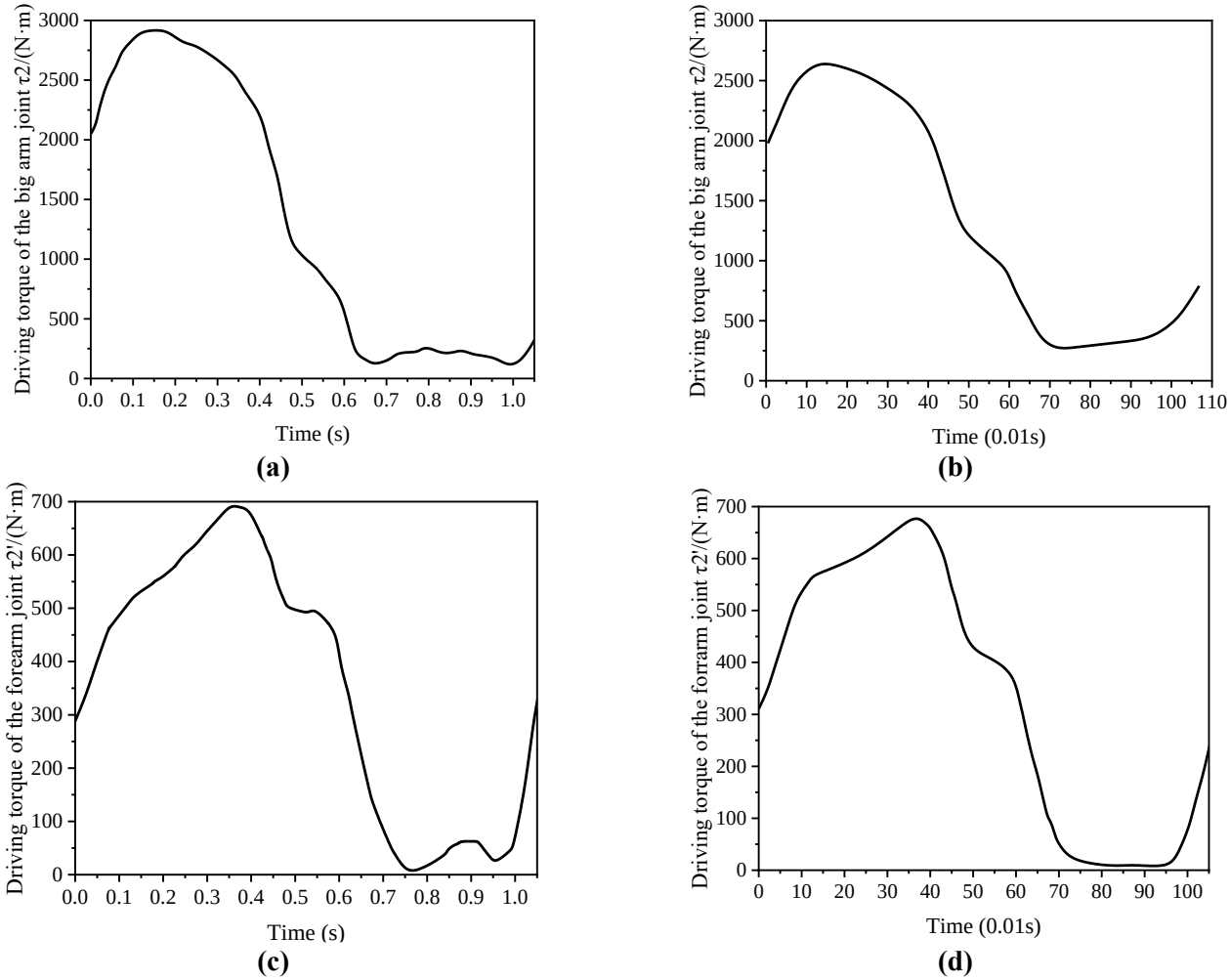

Figure 5. Comparison of simulation results of driving torque of the upper arm and the lower arm **(a)** big arm motor torque curve (SolidWorks motion); **(b)** big arm joint torque function curve (MATLAB); **(c)** forearm motor torque curve (SolidWorks Motion); **(d)** forearm joint torque function curve (MATLAB).

It can be seen from the comparison results that the joint torque function curve obtained by MATLAB simulation basically fits the motor torque curve obtained by SolidWorks Motion simulation. The peak driving torque of the large arm is 0.12 s, which is about 2900 $\mathrm{N \cdot m}$, and the peak driving torque of the lower arm is 0.36 s, which is about 700 $\mathrm{N \cdot m}$. It is proved that the dynamics theory of PR1300 stacking robot in this paper is correct and the simulation model is reasonable. The difference in some data may be caused by the omission of some parts during simulation.

5. Summary

In this paper, Kane method is used to study the inverse dynamics of 4-DOF stacking robot with closed chain structure. The main conclusions are as follows: (1)

The robot rod is divided into left and right branch chains, and the relationship between the generalized rate and the non-generalized rate of the system is obtained according to the forward kinematics solution. On this basis, fully considering the effect of the closed chain structure on the torque of the drive shaft, Kane method was used to program the PR1300 stacking robot to obtain the dynamic expression, which is a first-order differential algebraic equation set, and completely included the dynamic calculation of each moving component. Therefore, this model has practical guiding significance for the subsequent control strategy research and simulation. (2) The virtual prototype model was established in SolidWorks environment, and the dynamics simulation of the stacking robot was carried out based on the SolidWorks Motion simulation platform under the premise of given motion path and motion law, and the driving torque curve of the upper and lower arm joints was obtained. Compared with the simultion results of theoretical model using MATLAB. The comparison results show that the kinetic theory is correct and the simulation model is reasonable. Both the software simulation and the numerical calculation show that the 4-DOF stacking robot with closed chain structure moves smoothly and has no strong impact on the motor due to the interaction between different components, which provides the necessary basis for the dynamic scale synthesis of subsequent robots.

Author contributions: Conceptualization, LY and RJ; methodology, LY; software, LY; validation, LY, RJ and MZ; formal analysis, LY; investigation, LY; resources, LY; data curation, LY; writing—original draft preparation, LY; writing—review and editing, LY; visualization, MZ; supervision, MZ; project administration, MZ; funding acquisition, MZ. All authors have read and agreed to the published version of the manuscript.

Acknowledgments: This work was financially supported by key projects of natural science research in universities in Anhui province (2023AH051559).

Ethical approval: Not applicable.

Conflict of interest: The authors declare no conflict of interest.

References

1. Ho Vinh Nguyen, Vo Duy Cong, Phan Xuan Trung. Development of a SCARA Robot Arm for Palletizing Applications Based on Computer Vision[J]. FME TRANSACTIONS. 2023, 51(4):10-20.
2. Park Il Hwan, Hong Dae Sun. Selection of Motors and Gear Reducers for Four-Axis Palletizing Robots Considering the Motion Characteristics and Dynamic Coupling Effect[J]. International Journal of Precision Engineering and Manufacturing. 2023, 24(12): 2269-2278.
3. Sun Huihui, Zhang Yujie, Xie Bin, Zi Bin. Dynamic Modeling and Error Analysis of a Cable-Linkage Serial-Parallel Palletizing Robot[J]. IEEE ACCESS. 2021, 9: 2188-2200.
4. Chuang Yun-Ju, Chang Ho, Sun Yin-Tung, Tsung, Stick–slip in hand guidance of palletizing robot as collaborative robot[J]. International Journal of Advanced Robotic Systems. 2022, 19(5):1-12.
5. Cheng, S., Argaud, JP., Iooss, B. et al. A Graph Clustering Approach to Localization for Adaptive Covariance Tuning in Data Assimilation Based on State-Observation Mapping[J]. Math Geosci.2021, 53:1751–1780
6. Gong, HL., Li, H., Xiao, D. et al. Reactor field reconstruction from sparse and movable sensors using Voronoi tessellation-assisted convolutional neural networks[J]. NUCL SCI TECH. 2024, 35, 43.
7. Sibo Cheng, Yilin Zhuang, Lyes Kahouadji. et al.Multi-domain encoder–decoder neural networks for latent data assimilation in dynamical systems[J]. Computer Methods in Applied Mechanics and Engineering, 2024, 430: 117201.

8. ZENG Q, FANG Y. Structural synthesis and analysis of serial-parallel hybrid mechanisms with spatial multi-loop kinematic chains[J]. Mechanism and Machine Theory. 2012, 49: 198-215.
9. SHEN H P, ZHAO H B, DENG J M, et al. Type design method and the application for hybrid robot based on freedom distribution and position and orientation characteristic set[J]. Journal of Mechanical Engineering. 2011, 47(23): 56 -64.
10. Xiu Shu Han, Qiang Tian. Kinematics Analysis of Palletizing Robot[J]. Advanced Materials Research. 2014, 3140(915): 477-481.
11. GUO W J, LI R F, CAO C Q, et al. Kinematics analysis of a novel 5-DOF hybrid manipulator[J]. International Journal of Automation Technology. 2015, 9(6): 765 -774.
12. Lin Jian Liang, Xue Guan Gao. Palletizing Robot Dynamic Analysis and Simulation[J]. Applied Mechanics and Materials. 2014, 3342 (598): 623-626.
13. Song Zhenwei, Sun Yuzhong, Wang Shaoqi, et al. Joint Simulation Analysis of Stacking Robot Based on UG NX and PLC[J]. MECHANICAL & ELECTRICAL ENGINEERING TECHNOLOGY. 2024, 53(4):86-91.
14. LI Yanbiao, ZHENG Huang, CHEN Bo, et al. Dynamic modeling and analysis of 5-PSS/UPU parallel mechanism with elastically active branched chains[J]. Chinese Journal of Mechanical Engineering. 2020, 33: 118-129.
15. YAO Jiantao, GU Weidong, FENG Zongqiang, et al. Dynamic analysis and driving force optimization of a 5-DOF parallel manipulator with redundant actuation[J]. Robotics and Computer-Integrated Manufacturing. 2017, 48: 51-58.
16. CHEN Genliang, YU Weidong, LI Qinchuan, et al. Dynamic modeling and performance analysis of the 3-PRRU 1T2R parallel manipulator without parasitic motion[J]. Nonlinear Dynamics. 2017, 90(1): 339-353.
17. CHEN Miao, ZHANG Qing, QIN Xianrong, et al. Kinematic, dynamic, and performance analysis of a new 3-DOF over-constrained parallel mechanism without parasitic motion[J]. Mechanism and Machine Theory. 2021, 162: 104365.
18. LI Yanbiao, ZHENG Huang, CHEN Bo, et al. Dynamic modeling and analysis of 5-PSS/UPU parallel mechanism with elastically active branched chains[J]. Chinese Journal of Mechanical Engineering. 2020, 33: 118-129.
19. LIU W, GONG Z, WANG Q. Investigation on Kane dynamic equations based on screw theory for open-chain manipulators[J]. Applied Mathematics and Mechanics. 2005, 26(5): 627-635.
20. CHENG G, SHAN X. Dynamics analysis of a parallel hip joint simulator with four degree of freedoms (3R1T) [J]. Nonlinear Dynamics. 2012, 70(4): 2475 -248.
21. ZHANG Dongsheng, XU Yundou, YAO Jiantao, ZHAO Yongsheng. Inverse Dynamic Analysis of Novel 5-DOF Hybrid Manipulator[J]. Transactions of the Chinese Society for Agricultural Machinery. 2017, 48(9):385-393.
22. WU Jun, WANG Jinsong, WANG Liping. Identification of dynamic parameter of a 3DOF parallel manipulator with actuation redundancy[J]. Journal of Manufacturing Science and Engineering. 2008, 130(4): 041012.
23. ZHANG Huizhen, CHANG Gang, SHAN Xianlei, et al. Singularity-free path optimization of the parallel test mechanism for artificial hip joints[J]. Journal of Mechanical Science and Technology. 2018, 32(4):1775-1786.
24. Y. He, J. Mei, Z. Fang, F. Zhang, Y. Zhao. Minimum Energy Trajectory Optimization for Driving Systems of Palletizing Robot Joints[J]. Mathematical Problems in Engineering. 2018, 1:7247093.
25. A. Martini, M. Troncossi, A. Rivola. Algorithm for the static balancing of serial and parallel mechanisms combining counterweights and springs: Generation, assessment and ranking of effective design variants[J]. Mechanism and Machine Theory. 2019, 137: 336-354.